Mineralogy and Petrology (2002) 76: 195–212

Mineralogy and Petrology



# Cathodoluminescence (CL) and electron paramagnetic resonance (EPR) studies of clay minerals

**J. Götze**[1], **M. Plötze**[2], **Th. Götte**[3], **R. D. Neuser**[3], and **D. K. Richter**[3]

[1] Department of Mineralogy, TU Bergakademie Freiberg, Federal Republic of Germany
[2] Department of Geotechniques, ETH Zürich, Switzerland
[3] Department of Geology, Mineralogy and Geophysics, Ruhr-University Bochum, Federal Republic of Germany

Received December 3, 2001; revised version accepted February 27, 2002
Editorial handling: A. Finch

**Summary**

Sheet silicates of the serpentine–kaolin-group (serpentine, kaolinite, dickite, nacrite, halloysite), the talc–pyrophyllite-group (talc, pyrophyllite), the smectite-group (montmorillonite), and illite (as a mineral of the mica-group) were investigated to obtain information concerning their cathodoluminescence behaviour. The study included analyses by cathodoluminescence (CL microscopy and spectroscopy), electron paramagnetic resonance (EPR), X-Ray diffraction (XRD), scanning electron microscopy (SEM) and trace element analysis.

In general, all dioctahedral clay minerals exhibit a visible CL. Kaolinite, dickite, nacrite and pyrophyllite have a characteristic deep blue CL, whereas halloysite emission is in the greenish-blue region. On the contrary, the trioctahedral minerals (serpentine, talc) and illite do not show visible CL.

The characteristic blue CL is caused by an intense emission band around 400 nm (double peak with two maxima at 375 and 410 nm). EPR measurements indicate that this blue emission can be related to radiation induced defect centres (RID), which occur as electron holes trapped on apical oxygens (Si–O centre) or located at the Al–O–Al group (Al substituting Si in the tetrahedron). Additional CL emission bands were detected at 580 nm in halloysite and kaolinite, and between 700 and 800 nm in kaolinite, dickite, nacrite and pyrophyllite.

Time-resolved spectral CL measurements show typical luminescence kinetics for the different clay minerals, which enable differentiation between the various dioctahedral minerals (e.g. kaolinite and dickite), even in thin section.

## Introduction

Clay minerals are an important constituent of sediments and sedimentary rocks, and also occur as alteration products in crystalline rocks. Because of their widespread occurrence, and their physical and chemical properties, clay minerals are widely used in certain technical applications (e.g. ceramics, filling materials, refractory materials, geotechnical engineering). On the other hand, clay minerals are important minerals in sedimentary petrology as indicators of specific facies conditions in different geological environments (e.g. *Bailey*, 1988).

During the last few years, the advantages of cathodoluminescence (CL) in several applications in the geosciences (e.g. *Pagel* et al., 2000) have resulted in an increasing interest in the luminescence properties of clay minerals. Despite numerous investigations of clay minerals, no information concerning their general luminescence behaviour exists. It was assumed that kaolinite and dickite are the only clay minerals which exhibit visible CL. Excited by an electron beam, kaolinite shows a characteristic deep blue CL, which enables it to be distinguished from other minerals (*Marshall*, 1988). In the present work, an investigation by CL microscopy and spectroscopy complemented by electron paramagnetic resonance (EPR), X-ray diffraction (XRD), trace-element analysis and scanning electron microscopy (SEM) provides more information concerning the real structure and luminescence behaviour of the most important clay minerals.

## Materials and methods

Representatives of different groups of clay minerals were selected for the present reconnaissance study. The material includes clay mineral samples from different localities around the world and of different genesis (sedimentary, diagenetic, hydrothermal). The selected mineral groups are the serpentine–kaolin-group (serpentine, kaolinite, dickite, nacrite, halloysite), the talc–pyrophyllite-group (talc, pyrophyllite), the smectite-group (montmorillonite), and illite as a representative mineral from the mica-group (Table 1).

The mineralogical composition and the crystal structure of the investigated clay samples was characterized by XRD (BRUKER-AXS D8; CuK$\alpha$; 4–70° 2, 0.02° steps, 3 s per step) using Rietveld refinement (AutoQuan/BGMN). The material was additionally studied by SEM (JEOL 6400) to detect variations in grain size and morphology of the different minerals. CL investigations were carried out on carbon-coated polished thin sections of the clay mineral samples or clay-bearing rocks, which were prepared using low-fluorescing epoxy resin. We used a ''hot cathode'' CL microscope at 14 kV and with a current density of $\sim 10\,\mu A\,mm^{-2}$ (*Neuser* et al., 1995). The analyses were performed for all samples except montmorillonite, where a preparation of polished thin sections was impossible. To prevent contamination from the used epoxy resin on the spectral CL measurements, tablets of pressed powder samples were additionally made using a hydraulic press at 10 t.

Luminescence images were captured ''on-line'' during CL operations using an adapted digital video camera (KAPPA 961-1138 CF 20 DXC with cooled CCD). Cathodoluminescence spectra were obtained using an EG&G digital triple-grating spectrograph with a liquid nitrogen cooled CCD detector in the range

Table 1. *Origin of investigated clay mineral samples of the present study*

| Mineral | Sample | Locality | Origin |
|---|---|---|---|
| Kaolinite | KGa-1 | Washington county, USA | sedimentary<br>*CMS source clay* |
| | KGa-2 | Warren county, USA | sedimentary<br>*CMS source clay* |
| | KNak-1 | Rochlitz, Germany | hydrothermal<br>(so called ''Steinmark'') |
| | KAug | Augustusburg, Germany | altered rhyolite |
| | Tovo-3 | Bahratal, Germany<br>Niederschöna layers | diagenetic cement in<br>Cretaceous sandstone |
| Dickite | KDick-1 | Barkly, South Africa | hydrothermal |
| | KDick-P | Huaraz, Peru | hydrothermal |
| | KDick-M | San Juanito, Chihuahua/Mexico | hydrothermal |
| | RöTo-204 | Altenberg, Germany | hydrothermal |
| | K-$C_1$WL | Königstein borehole, Germany<br>Niederschöna layers | diagenetic cement in<br>Cretaceous sandstone |
| Nacrite | KNak-2 | Flöha, Germany | hydrothermal |
| | RöTo-203 | Sidi Amar, Tunisia | hydrothermal |
| | KNak-3 | Freiberg, Germany | hydrothermal |
| Halloysite | KHal-1 | Entre-Sambre-et-Meuse, Belgium | karst formation |
| | KHal-2 | Djebel Debar, Algeria | sedimentary |
| Pyrophyllite | KPyr-1 | Recht, Belgium | hydrothermal |
| | KPyr-2 | Robbins, North Carolina/USA | hydrothermal |
| | KPyr-3 | Beresowsk, Ural/Russia | hydrothermal |
| | KPyr-4 | Witwatersrand, R.S.A. | hydrothermal |
| Illite | Illite-S | Sárospatak, Hungary | hydrothermal |
| | Illite-M | Monte Casslano, Switzerland | sedimentary, metamorphic |
| Montmorillonite | SWy-1 | Crook county, Wyoming/USA | alteration of volcanic ash<br>*CMS source clay* |
| | STx-1 | Gonzales county, Texas/USA | alteration of volcanic ash<br>*CMS source clay* |
| | SAz-1 | Cheto, Apache county, Arizona | alteration of vitric tuff<br>*CMS source clay* |
| | Vol | Volclay, Wyoming | alteration of volcanic ash |
| | MX80 | Wyoming (Süd-Chemie, Bavaria) | alteration of volcanic ash |
| Serpentine | Ser-1 | Snarum, Norge | |
| Talc | Talc-1 | Cuba | |

380–1000 nm (VIS-IR). To prevent distortion of the spectra by prolonged exposure to the electron beam, all spectra were taken on non-irradiated sample spots. Time-resolved ($10 \times 20$ s) CL spectra were measured on selected samples to study the CL behaviour of the minerals during electron irradiation. In addition, spectral CL investigations were carried out using a JEOL JSM 6400 SEM equipped with an Oxford MonoCL system. For CL investigations, the accelerating voltage was set at 20 kV and the beam current in the range 0.6–1.6 nA. The CL spectra were detected

over the range 200–800 nm (UV-VIS), with 1 nm steps and a dwell time of 1 s per step.

For the identification of point defects in the crystal structure of the clay minerals, paramagnetic centres were investigated in powder samples by EPR (BRUKER ESP 300 E) in the X-band at 295 and 70 K (5 G, 40 mW, 100–200 mT and 320–336 mT). For the investigation of the irradiation dependent behaviour of radiation induced point defects (RID), the clay samples were irradiated using a $^{60}$Co irradiation chamber with a dose rate of 2.548 kGy h$^{-1}$ (total dose 1.1 MGy) as powders in the presence of air at room temperature. Additionally, the trace-element content of selected clay samples was determined by Inductively Coupled Plasma Mass Spectrometry (ICP-MS Agilent 7500).

## Results and discussion

### *Mineralogy and trace element composition of the clay mineral samples*

The results of XRD and Rietveld analysis of the impure material show that except for some dickites all samples contain other phases (Table 2). This must be considered for the interpretation of data. It can not be excluded that some signals in the bulk samples come from impurity phases (e.g. EPR signals of RID in montmorillonite may be caused by quartz impurities, which show similar parameters).

Table 2. *XRD Rietveld analysis of investigated clay minerals (semi-quantitative for smectite samples)*

| Sample | Mineralogy of the clay samples (non-purified) | |
|---|---|---|
| KGa-1 | 97% kaolinite, 2.5% anatase, 0.5% crandallite | **Hinckley index 0.93** |
| KGa-2 | 95.5% kaolinite, 4% anatase, 0.5% crandallite | **Hinckley index 0.35** |
| KNak-1 | 99% kaolinite, 1% anatase, feldspar | **Hinckley index 0.69** |
| KDick-1 | 100% dickite | |
| KDick-M | 43% dickite, 57% nacrite | |
| KDick-P | 100% dickite | |
| RöTo-204 | 100% dickite | |
| KNak-2 | nacrite + ? | |
| RöTo-203 | 65% illite, 25% pyrophyllite, 5% nacrite, 5% feldspar, kaolinite | |
| KHal-1 | metahalloysite, kaolinite, traces quartz, chlorite | |
| KHal-2 | halloysite, kaolinite, traces quartz, illite(?) | |
| KPyr-2 | 70% pyrophyllite, 25% illite, 5% serpentine | |
| Illite-M | 95% illite, 3% quartz, 2% feldspar | |
| Illite-S | 90% illite + ml, 5% quartz, 2% feldspar, amorphous | |
| SAz-1* | 98% Ca-smectite, 1% quartz, traces feldspar, mica, magnetite | |
| STx-1* | 67% Ca-smectite, 30% opal-CT, 3% quartz, traces kaolinite, feldspar | |
| SWy-1 | 70% Na-smectite, 15% feldspar, 10% quartz, 5% calcite, cristobalite, illite | |
| MX-80** | 75% Na-smectite, 15% quartz, 8% feldspar, 1% calcite, traces mica, kaolinite, cristobalite, pyrite | |
| Vol | 79% Na-smectite, 10% quartz, 10% feldspar, 1% gypsum | |

*CMS values from *Chipera* and *Bish* (2001) and **_Müller-Vonmoos_ and _Kahr_ (1983)

In sample RöTo-203, for instance, only some of the bulk material is really nacrite, which has to be considered during CL measurements.

The mineralogical and geochemical characterization of the investigated clay minerals illustrates that the samples differ significantly in grain size and morphology of the crystals, crystallinity (compare Hinckley indices in Table 2) or trace element composition (Table 3). The two kaolinite samples KGa-1 and KGa-2 show very similar trace-element contents, except Fe, Li, Zn and Pb. The high content of iron in kaolinite sample KGa-2 and the higher value of Th (from the CMS source clay sample KGa-1b) in particular should influence the luminescence behaviour. Iron acts as a luminescence quencher and Th leads to the formation of radiation induced defect centres which are probably responsible for CL (*Marfunin*, 1979).

Differences in the trace-element composition of the dickite samples may especially be detected for the elements Ca, Sr and Ba, which are significantly low in sample KDick-1 and elevated in KDick-P. Elements relevant as potential activators or quenchers of luminescence are enriched in sample KDick-1 (Mn, Cu) and KDick-M (Fe, Pb) respectively. The high iron content in sample K-DickP is due to iron oxides, since no elevated concentrations of $Fe^{3+}$ centres were detected by EPR measurements. The appreciable K content in the nacrite sample RöTo-203 reflects the presence of illite, as indicated also in the XRD patterns.

XRD results are consistent with SEM analyses that reveal significant variations in grain size and morphology of the investigated minerals, as shown for selected samples in Plate 1. For instance, the poorly crystalline kaolinite from Warren county (Hinckley index 0.35), as well as the halloysite and illite samples, are characterized by randomly oriented fine plates ($<1\,\mu m$), whereas the almost perfect crystallized kaolinite KGa-1 (Hinckley index 0.93) has a mean grain size of 5 μm (Table 2, Plate 1). The high index value of 0.93 for sample KGa-1 reflects the low defect density of this sample, whereas the values of 0.69 for sample KNak-1 and 0.35 for KGa-2, respectively, are characteristic of medium- to high-defect densities (*Hinckley*, 1963). Kaolinite and dickite cements from sandstones (e.g., Königstein borehole, Bahratal – see Plate 1b and d) exhibit well crystallized "books". In contrast, the dickite sample from South Africa mainly consists of lath-shaped euhedral crystals of 20–80 μm size (Plate 1c), whereas the nacrite and pyrophyllite samples in general show flaky crystals with crystal sizes partially $>100\,\mu m$ (Plate 1e and g).

### *CL microscopy*

Despite the detected variations of mineralogical properties, the CL results revealed for the first time that all dioctahedral minerals of the serpentine–kaolin-group (kaolinite, dickite and nacrite) exhibit a deep blue luminescence under electron irradiation (Plate 2). This emission has been also detected in the dioctahedral three-layer mineral pyrophyllite. The CL of halloysite is relatively weak with a greenish-blue tint. With that, these minerals can easily be distinguished from the trioctahedral sheet silicates (serpentine and talc) and illite (all with no visible CL). No illite samples with visible CL were found. Only red CL of muscovite and weak blue CL of lepidolite have been reported (*Görz* et al., 1970; *Weber*, 2000; *Rene* et al., 2001).

Table 3. *Trace element composition of selected clay mineral samples (results in ppm)*

| Element | KGa-1 kaolinite | KGa-2 kaolinite | KDick-1 dickite | KDick-M dickite | KDick-P dickite | KHal-1 halloysite | KHal-2 halloysite | RöTo-203 nacrite | Illite-S$^{+}$ illite | STx-1$^{*}$ Ca-smectite | SAz-1$^{*}$ Ca-smectite | MX-80$^{**}$ Na-smectite | Vol Na-smectite |
|---|---|---|---|---|---|---|---|---|---|---|---|---|---|
| Li | 6.4 | 83 | 27 | 81 | 100 | 7.4 | 7.5 | 2.1 | na | na | na | na | na |
| Na | 150 | 78 | 54 | 73 | 62 | 230 | 270 | 3410 | 334 | 1150 | 223 | 111 | 7420 |
| K | 280 | 350 | 30 | 220 | 330 | 560 | 810 | 47680 | 32785 | 291 | 788 | 415 | 2490 |
| Rb | 1.1 | 1.8 | 0.2 | 0.2 | 0.1 | 1.9 | 2.6 | 240 | na | 3.8 | 4.2 | na | na |
| Mg | 24 | 60 | 51 | 4.6 | 1.5 | 58 | 56 | 26 | 9045 | 22854 | 40582 | 14351 | 15678 |
| Ca | 260 | 200 | 230 | 950 | 1350 | 920 | 1300 | 120 | 5720 | 12370 | 22522 | 13084 | 3575 |
| Sr | 20 | 36 | 0.8 | 610 | 1070 | 51 | 77 | 33 | na | 81.7 | 304.2 | na | na |
| Ba | 35 | 80 | 6.1 | 340 | 650 | 920 | 920 | 380 | na | na | na | na | na |
| Fe | 930 | 4810 | 240 | 1300 | 170 | 620 | 620 | 410 | 1049 | 4196 | 6190 | 13114 | 12239 |
| Mn | 3.1 | 9.4 | 160 | 1.2 | 3.0 | 46 | 67 | 1.5 | 232 | na | na | 15 | 77 |
| Ti$^{*}$ | 10011 | 11450 | na | na | na | na | na | na | 300 | 1559 | 1499 | traces | 779 |
| V | 180 | 100 | 27 | 130 | 100 | 1.3 | 1.9 | 24 | na | na | na | na | na |
| Cr | 73 | 82 | 1.8 | 24 | 22 | 4.2 | 3.7 | – | na | na | na | na | na |
| Co | 1.8 | 7.9 | 0.6 | 0.1 | – | 3.9 | 4.8 | – | na | 1.3 | 1.1 | na | na |
| Ni | 20 | 40 | 1.9 | 1.3 | 0.2 | 120 | 120 | – | na | 5.0 | 2.6 | na | na |
| Cu | 12 | 13 | 34 | 2.6 | 1.2 | 87 | 88 | 1.9 | na | 7.5 | 3.1 | na | na |
| Zn | 8.1 | 44 | 7.6 | 0.9 | 2.4 | 170 | 200 | 1.6 | na | na | na | na | na |
| Pb | 9.8 | 62 | 3.6 | 330 | 22 | 80 | 79 | 17 | na | 6.2 | 34.8 | na | na |
| Tl | – | – | – | – | – | 3.4 | 4.9 | 1.4 | na | 0.3 | 0.2 | na | na |
| U | 2.7 | 4.8 | – | 1.9 | 3.7 | 0.4 | 0.4 | 7.8 | na | 6.8 | 1.2 | na | na |
| Th$^{*}$ | 37.2 | 11.4 | na | na | na | na | na | na | na | 25.7 | 24.3 | na | na |
| Σ REE$^{*}$ | 189.6 | 21.4 | na | na | na | na | na | na | na | 250.3 | 211.5 | na | na |

(–) = below detection limit (Cr 0.9 ppm, Co 0.1 ppm, Ni 0.6 ppm, Tl 0.1 ppm, U 0.2 ppm), *na* not analyzed. $^{*}$CMS values from *Mermut* and *Cano* (2001) and *Kogel* and *Lewis* (2001). $^{**}$fraction $<0.2\,\mu m$, Ca-form (*Müller-Vonmoos* and *Kahr*, 1983). $^{+}$fraction $<0.2\,\mu m$ (*Müller-Vonmoos* et al., 1991)

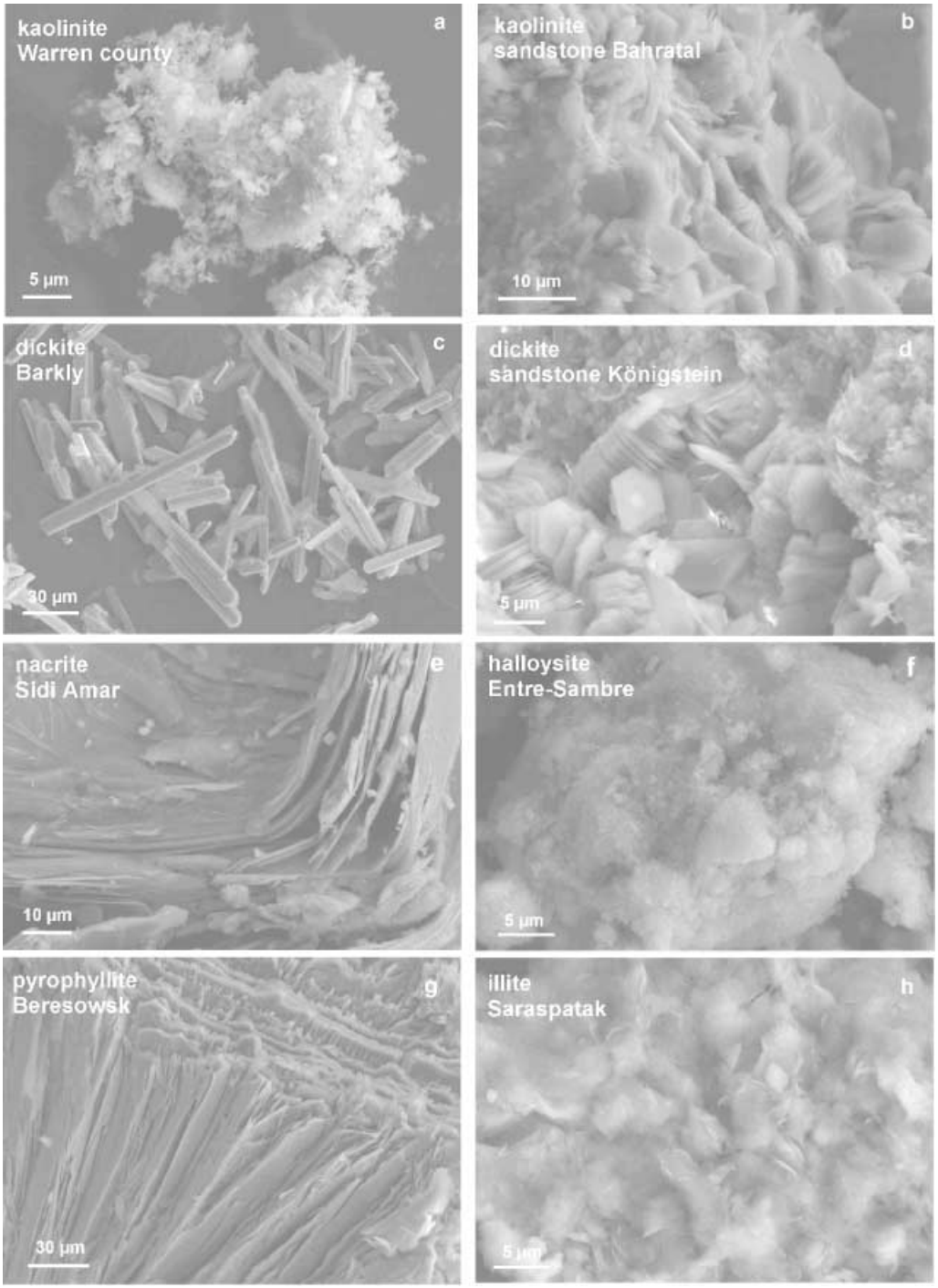


Plate 1. SEM micrographs of selected clay mineral samples. The secondary electron (SE) images illustrate the variations in grain size and morphology of the different sheet silicates

The characteristic blue CL of dioctahedral clay minerals enables the rapid detection of minor amounts of these minerals in geological and technical samples. For instance, kaolinization processes in small areas of rock samples are rapidly

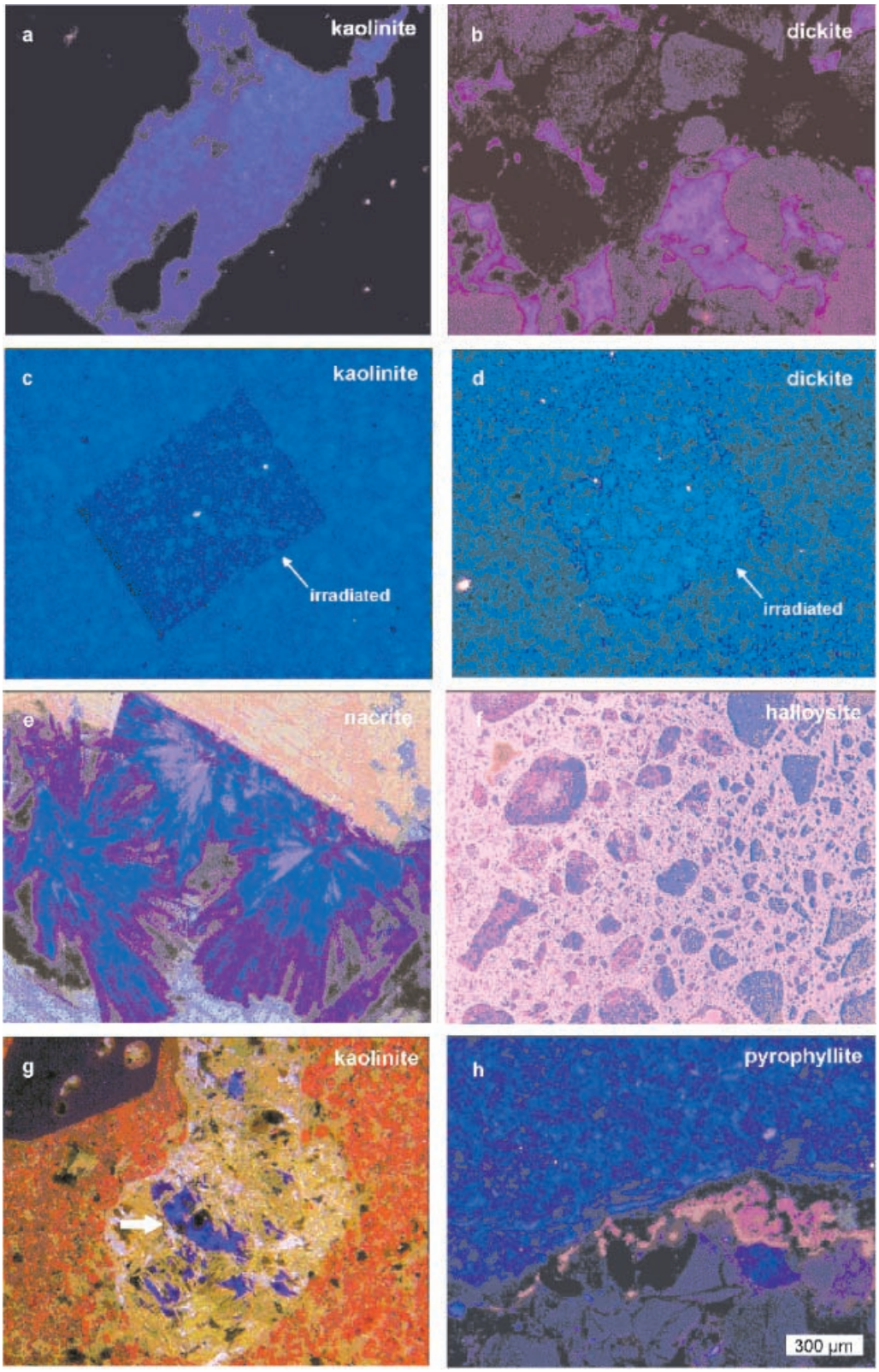
a
kaolinite
b
dickite
c
kaolinite
irradiated
d
dickite
irradiated
e
nacrite
f
halloysite
g
kaolinite
h
pyrophyllite
300 µm

detectable by CL (Plate 2g). The combination of CL microscopy and computer aided image analysis enables the quantification of the amount of luminescent cement material in sedimentary rocks (*Götze* and *Magnus*, 1997). Other examples illustrate that hydrothermal activities can also be revealed. For example Plate 2h shows a conglomerate sample from the Witwatersrand Au/U deposit, which was overprinted by hydrothermal fluids. The blue luminescent pyrophyllite enables detection of the areas of intense hydrothermal alteration.

*Spectral CL measurements*

The CL spectra of kaolinite, dickite, nacrite and pyrophyllite show, in general, very similar characteristics. The visible deep blue CL is caused by an emission band centred in the blue region at $\sim 400$ nm. Varying intensities of this emission band causes differences in the intensities of the visible blue CL (Plate 2). Spectral CL measurements with the SEM in the UV region of the spectrum revealed that the broad band emission around 400 nm is a double peak at the UV-VIS boundary consisting of two maxima at 375 nm and 410 nm (Fig. 1). In the spectra obtained with the CL microscope (OM-CL), only the 410 nm emission is visible. This is probably caused by the detector efficiency and additional absorption effects of the used glass optics.

A broad band emission between 700 and 800 nm was detected in samples of kaolinite, dickite, nacrite and pyrophyllite. The comparison of CL spectra obtained with SEM-CL and OM-CL (Figs. 1, 2), respectively, show a slight shift of the band maximum probably caused by differences in the detector efficiencies of the two rigs. The shape and half-width of the CL emission indicate that this broad band probably consists of at least two overlapping emissions (Fig. 1).

Plate 2. CL micrographs of selected samples illustrating the luminescence behaviour. **a** Pore space of a Cretaceous sandstone (Niederschöna layers, Bahratal, Germany) completely filled with blue luminescent kaolinite (sample Tovo3). The dark grains are detrital quartz grains. **b** Dickite cement in a Cretaceous sandstone (Niederschöna layers, Königstein, Germany) showing deep blue CL (sample K-C1WL). Note the corrosion of the detrital quartz grains by dickite. **c** Kaolinite sample KGa-1 from Washington county (USA) showing an dark ''window'', which is caused by electron irradiation with the SEM. The micrograph illustrates the decreasing CL intensity due to electron bombardment in kaolinite. **d** Dickite sample from Barkly, South Africa (KDick1) showing a ''window'' with enhanced CL intensity due to irradiation by an electron beam. The CL image emphasizes the increasing CL intensity during electron bombardment. **e** CL image of a nacrite sample from Flöha, Germany (KNak2) showing the typical shape of the crystals and the deep blue CL colour. **f** Aggregates of halloysite from Djebel Debar, Algeria (sample KHal2) with dull greenish-blue CL (doubled exposure time in comparison with the other samples). The material between the halloysite is the epoxy resin used for preparation of the thin sections. **g** Kaolinized plagioclase (arrow) within a rhyolite sample from Rochlitz, Germany. The alteration is only visible under CL due to the bright blue CL of the kaolinite. **h** Pyrophyllite within a quartz conglomerate sample from Witwatersrand, South Africa (sample KPyr-4) showing deep blue CL. The sample contains corroded quartz grains

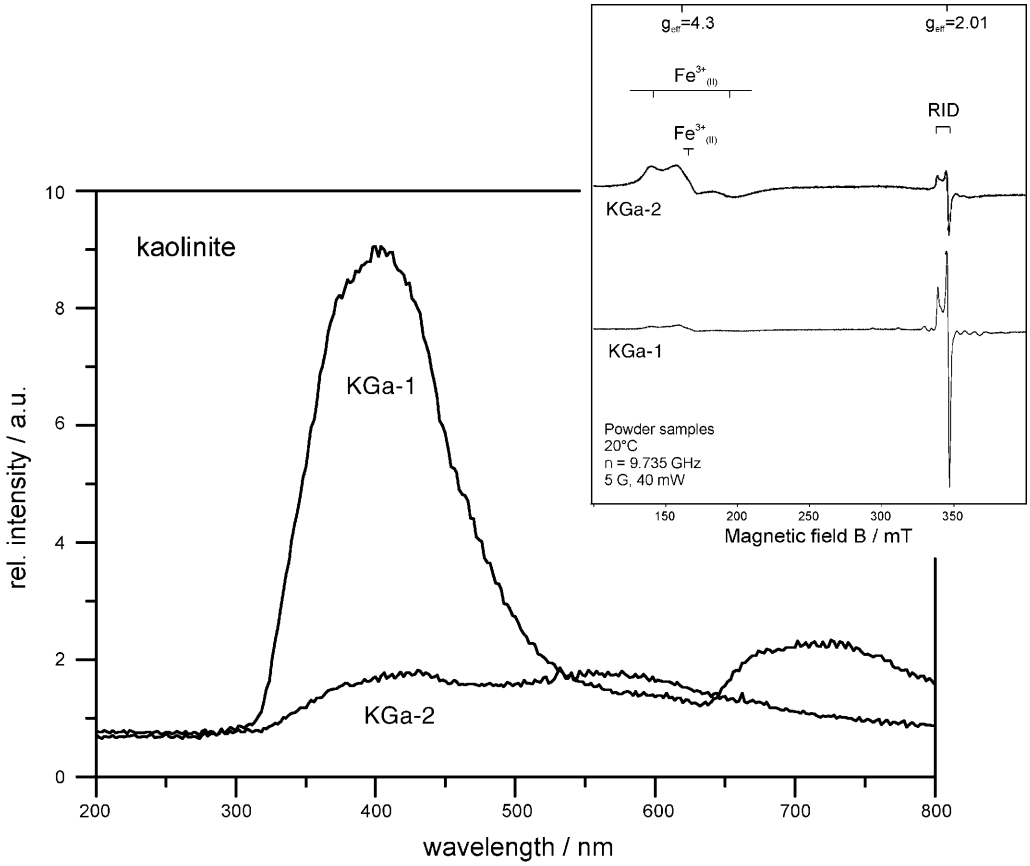


Fig. 1. Comparison of CL spectra (SEM-CL) and EPR spectra (inset) of kaolinite samples KGa-1 and KGa-2. The high intensity of the blue emission band in KGa-1 can be related to high contents of electron-hole centres (RID) in this sample. The broad band consists of two peaks centred at 375 nm and 410 nm, respectively. In contrast, sample KGa-2 has very low concentrations of RID centres and high concentrations of $Fe^{3+}$ centres. The broad emission band in the red/IR between 650 and 800 nm probably consists of at least two overlapping bands

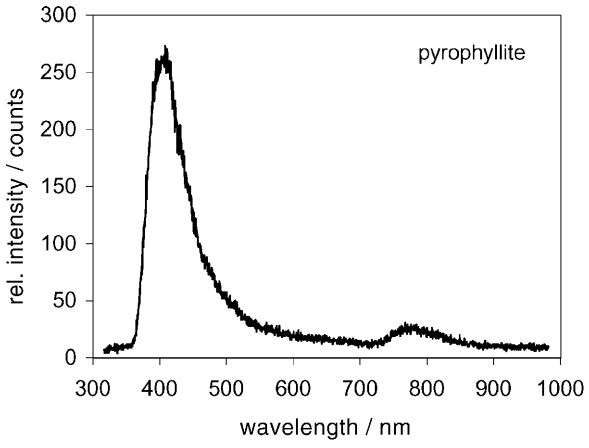


Fig. 2. CL emission spectrum (OM-CL) of a pyrophyllite sample showing the dominant blue emission band and an additional emission at $\sim$780 nm of unknown origin. Note that the emission in the red at the edge to the IR is slightly shifted in comparison with the SEM-CL spectrum in Fig. 1

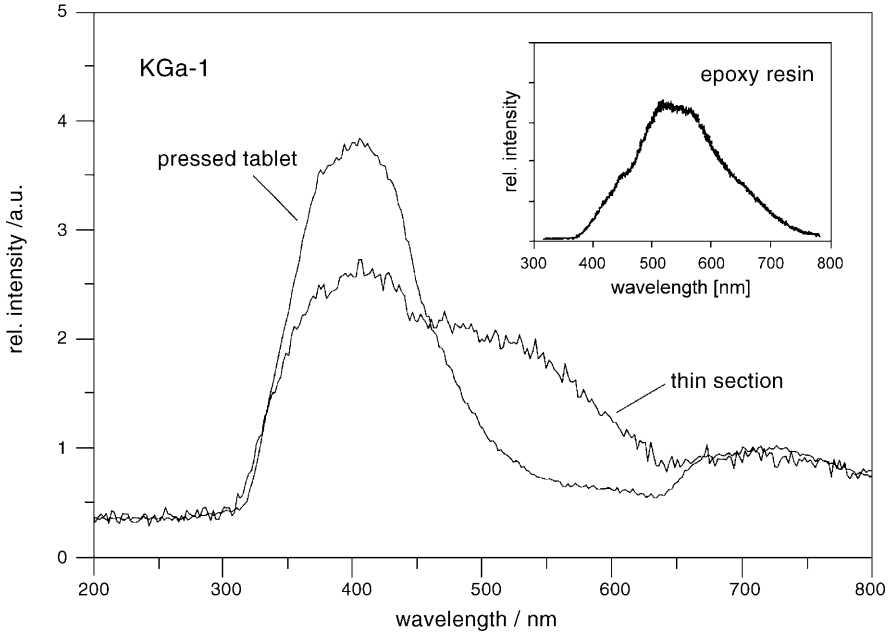


Fig. 3. SEM-CL spectra of kaolinite sample KGa-1 showing the effect of sample preparation. The thin section analysis shows background effects, lower intensity of the main blue emission band and an additional emission band between 450 and 650 nm, which can be related to the influence of the epoxy resin. Preparation of pressed tablets of kaolinite powder prevents the influence of the epoxy resin. The spectra were taken under the same experimental conditions (20 kV, 5.2 nA, enlargement 200x)

Some of the investigated clay mineral samples had additional emissions in the spectral region between 450 and 650 nm. Experimental data verified that this CL emission can in most cases be related to the influence of the epoxy resin used for the preparation of powder samples. The resin itself exhibits a broad and complex CL emission in this region (Fig. 3). To prevent the influence of the epoxy resin on the spectral CL measurements, we prepared pressed tablets of the powder samples with a hydraulic press. These tablets were studied by spectral CL measurements performed on a SEM. Figure 3 shows the comparison of the CL spectra of sample KGa-1, which were taken under constant experimental conditions from a conventional polished thin section and a pressed tablet, respectively.

Although we could confirm that the CL emissions in the region 450–650 nm in most of the fine-grained clay mineral samples were artefacts resulting from the epoxy resin, halloysite and the poorly crystalline kaolinite KGa-2 exhibit ''real'' CL emissions in this spectral region (Fig. 4). The CL spectra are very similar showing a very weak intensity of the characteristic blue emission and a main emission band centred at $\sim$ 580 nm. Although the origin of this CL emission is still unknown, it seems to be a characteristic feature of halloysite and poorly crystalline kaolinite.

*Time-resolved CL measurements*

To further investigate the kinetics of the different luminescence bands, the time-dependent intensities were measured during electron irradiation. Different

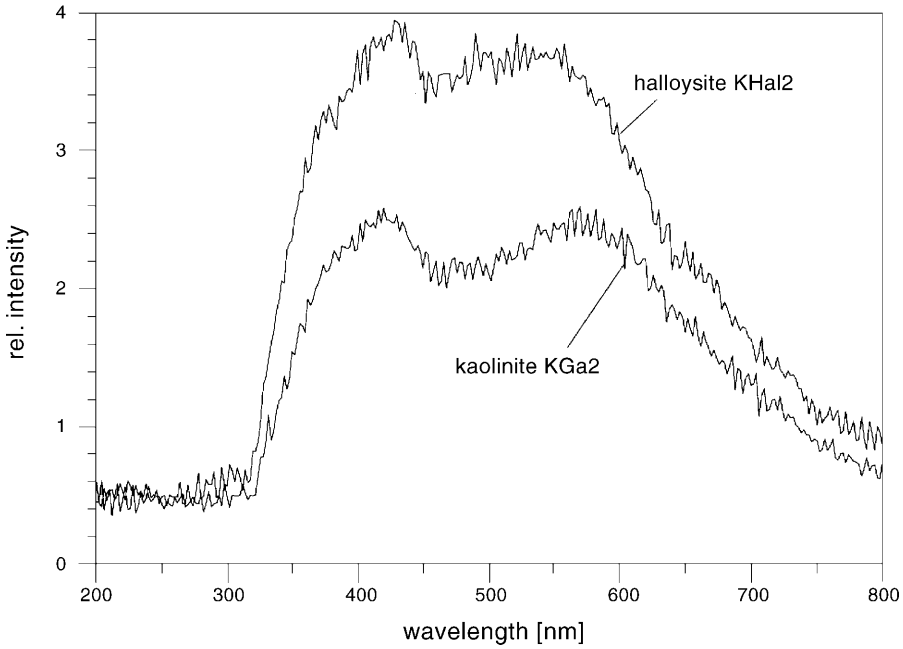


Fig. 4. CL spectra of kaolinite sample KGa-2 and halloysite KHal-2 taken on pressed tablets of the powder samples. The spectra show similar emission bands: (1) the typical blue emission at the UV-VIS boundary (weak double peak) and (2) a broad emission band with a maximum at $\sim$580 nm. The 410 nm emission in halloysite shows a intensity decrease during electron irradiation similar to that in kaolinite

irradiation-dependent intensity behaviour can be detected in the various clay minerals (Fig. 5). Kaolinite and halloysite show a transient behaviour with decreasing intensity of the blue emission band during electron irradiation independently of origin (sedimentary or hydrothermal) and crystalline order (*Götze* and *Plötze*, 2000). In contrast, the intensity of the blue CL of dickite, nacrite and pyrophyllite increases during CL measurements. This is clearly detectable in the time-resolved intensity curves of the 410 nm emission band (Fig. 5). The CL emission intensity of kaolinite rapidly decreases within 30–60 s of electron irradiation, whereas the CL emission intensities of dickite, nacrite and pyrophyllite strongly increase and then saturate after $\sim$150 s. This typical behaviour was detected in all samples investigated and enables differentiation between kaolinite and other dioctahedral clay minerals such as dickite, even in thin section.

Fig. 5. Time-dependent CL emission spectra of dioctahedral sheet silicates kaolinite, dickite, nacrite and pyrophyllite showing the development of the typical 410 nm emission during electron irradiation. Whereas the intensity of the CL emission intensity of kaolinite drastically decreases with irradiation time, the CL intensity of the other clay minerals strongly increases and saturates after about 150 s of electron bombardment. Despite the emission band around 550 nm in kaolinite, which is due to the luminescence of the epoxy resin used for preparation, all spectra are very similar

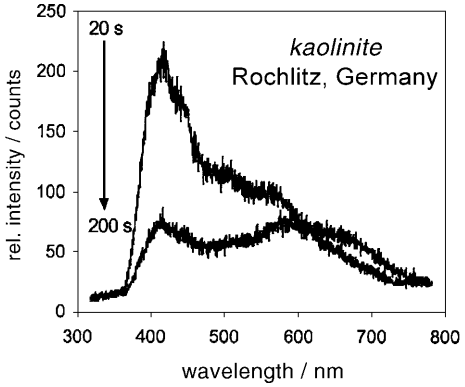
20 s
200 s
kaolinite
Rochlitz, Germany
rel. intensity / counts
wavelength / nm

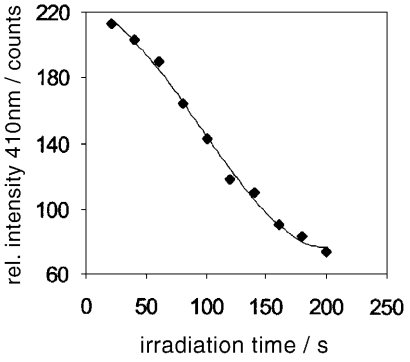
rel. intensity 410nm / counts
irradiation time / s

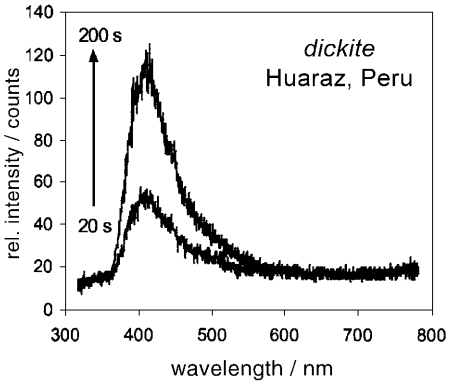
200 s
20 s
dickite
Huaraz, Peru
rel. intensity / counts
wavelength / nm

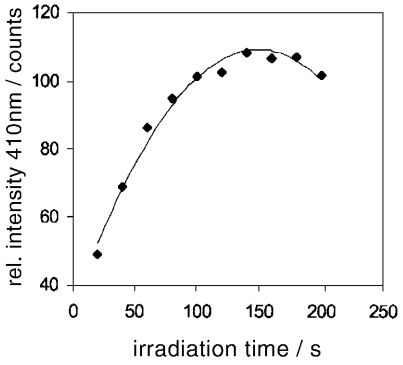
rel. intensity 410nm / counts
irradiation time / s

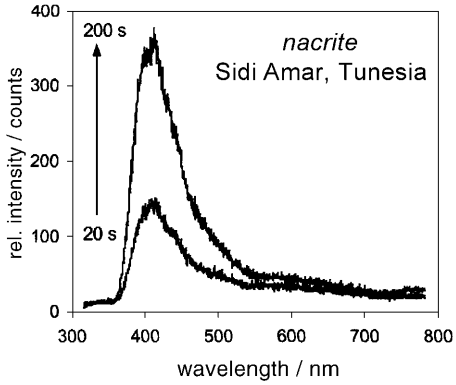
200 s
20 s
nacrite
Sidi Amar, Tunesia
rel. intensity / counts
wavelength / nm

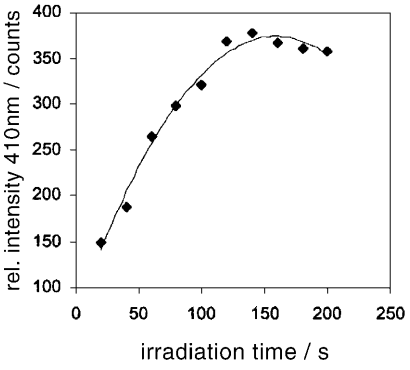
rel. intensity 410nm / counts
irradiation time / s

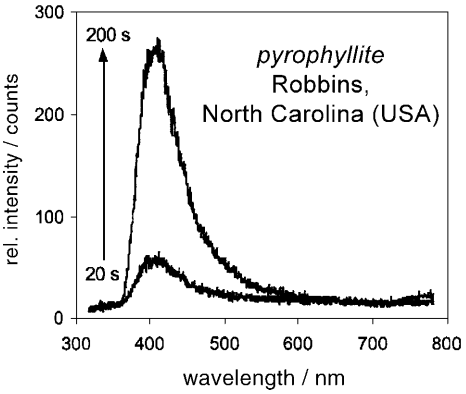
200 s
20 s
pyrophyllite
Robbins,
North Carolina (USA)
rel. intensity / counts
wavelength / nm

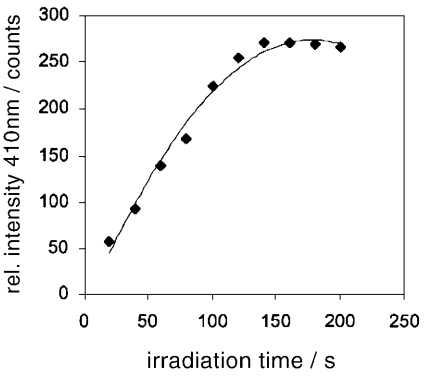
rel. intensity 410nm / counts
irradiation time / s

Plate 2c and d demonstrate this contrasting behaviour of the CL during electron irradiation by CL microscopy. The visible rectangles in the CL images of kaolinite and dickite are due to electron irradiation under the SEM before imaging. The samples show an opposite behaviour. The irradiated area in the kaolinite sample exhibits a decreased CL intensity, whereas it is easily detectable in dickite due to the enhanced CL intensity. Our results indicate, that these CL characteristics are independent of genesis, crystallinity, morphology or grain size of the minerals with the exception that well-crystallized kaolinite often shows a higher absolute CL intensity than poorly crystallized specimens.

The example of Cretaceous sandstones of the Niederschöna layers (samples Tovo3, K-C1WL) clearly demonstrates that neither a differentiation by simple CL imaging (Plate 2a/b) or by SEM (Plate 1b and d) is possible. In contrast, the time-resolved spectral CL measurements revealed that, for the identical stratigraphic position, the cement in sample Tovo3 is kaolinite and is dickite in K-C1WL. The latter probably results from hydrothermal overprint after deposition of the sediments accompanied by U mineralization.

*EPR spectroscopy and identification of luminescence activators*

Further results concerning the origin of the CL properties of the clay minerals investigated were obtained by EPR studies. By EPR, paramagnetic defects were detected in unirradiated and irradiated natural samples. The EPR spectra of kaolinite and other clay minerals usually consist of two regions, low-field resonance with $g = 3.5$–$4.9$, which is associated with $Fe^{3+}$ substituting for $Al^{3+}$, and high-field resonance with $g \sim 2.0$, which can be assigned to radiation-induced defects (RID) (*Clozel* et al., 1994).

$Fe^{3+}$ substitutes for $Al^{3+}$ at two octahedral positions causing the EPR spectra at $g_{\text{eff.}} \sim 4.3$ (*Meads* and *Malden*, 1975). These spectra could be found in almost all samples with different intensities (Fig. 6). The highest concentrations are in illite and montmorillonite and the lowest in dickite and nacrite samples. After $\gamma$-irradiation the intensity decreases due to the partial reduction of trivalent iron to the divalent (see also *Gournis* et al., 2000; *Plötze* and *Kahr*, 2001).

The other important group of paramagnetic centres represents the radiation induced paramagnetic defect centres (RID) with spectra at $g_{\text{eff.}} \sim 2.0$ (*Clozel* et al., 1994). These so-called 'A' centres are assigned to electron holes trapped on apical oxygens with different orientations (Si–O centres). The 'B' centre is assigned to an electron hole located at the Al–O–Al group (Al substituting Si in the tetrahedron) and shows an intense hyperfine structure (HFS) with $^{27}Al$ nuclei (especially in the spectra at 70 K). The signal intensity of both centres varies for different clay minerals. In illite and montmorillonite very weak signals of RID could be detected. However, it cannot be excluded that the signals are an artefact. In illite and montmorillonite, RID could not be detected. In the group of dioctahedral clay minerals, the highest concentrations of RID were measured in well crystallized kaolinite (Fig. 6), whereas halloysite has almost no RID. The dickite and nacrite samples have more B centres (Si–O) than A centres (Al–O–Al).

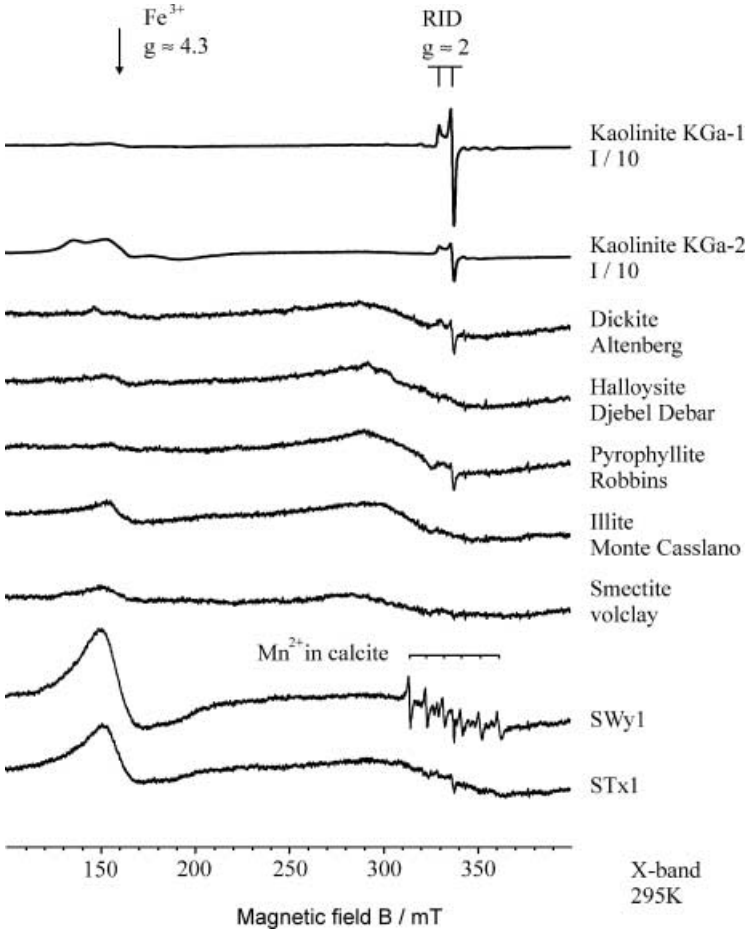


Fig. 6. EPR spectra (X band, 295 K) of selected clay minerals showing the differences in the concentrations of $Fe^{3+}$ and RID centres. The hyperfine structure in sample SWy1 is due to $Mn^{2+}$ from minor amounts of calcite in the sample

The comparison of EPR spectra with CL spectra indicates that the main CL emission band around 400 nm can probably be related to RID centres in the structure (Fig. 1). The two kaolinite samples KGa-1 and KGa-2 have quite different intensities of RID centres, which correlate well with the intensity of the blue CL emission. Sample KGa-1 with high concentrations of RID has a strong blue CL emission, whereas sample KGa-2 has low concentrations of RID and only a slight blue emission band.

The irradiation dependent CL behaviour of the dioctahedral clay minerals correlates with the behaviour of the RID centres during irradiation. After $\gamma$-irradiation the intensity of RID centres in kaolin group clay minerals strongly increases. The intensity of B centres increases more strongly than those of the A centres (Fig. 7). Only for kaolinite does the concentration of B centres slightly decrease. Assuming that the 410 nm CL emission band can be related to the Si–O centre, this would explain the increase of this band in dickite, nacrite and pyrophyllite, while the intensity of this CL emission decreases in kaolinite and halloysite.

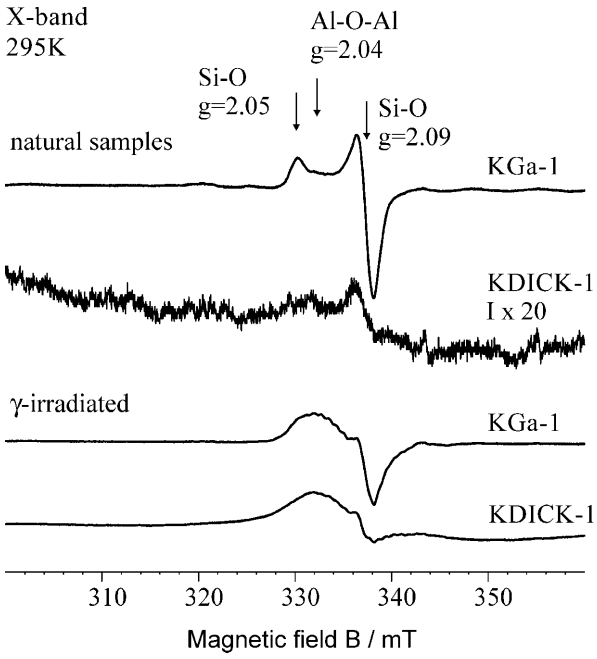


Fig. 7. Comparison of EPR spectra (X band, 295 K) of natural and $\gamma$-irradiated samples of kaolinite KGa-1 and dickite KDick-1. The concentration of Al–O–Al centres in both samples and Si–O centres in dickite increases during $\gamma$-irradiation, whereas the Si–O centre in kaolinite shows a decreasing intensity

In conclusion, the double peak in the CL emission of the dioctahedral clay minerals can probably be assigned to the two different types of RID centres, the Si–O and Al–O–Al centre. Variations in shape and position of the resulting broad band can probably be assigned to different populations of the two centre types. Further studies are currently in progress to clarify the relationship between the time-dependent CL behaviour and the radiation dependence of paramagnetic centres.

The relationship between $Fe^{3+}$ centres and possible CL activation or quenching effects is still unclear. The comparison of the CL spectra of the kaolinite samples KGa-1 and KGa-2 (Fig. 1) indicates that the emission in the red-IR is not caused by $Fe^{3+}$ activation as in feldspar. Sample KGa-2 has a much higher iron content (compare Table 3) and many more $Fe^{3+}$ centres than sample KGa-1 but no CL emission between 700 and 800 nm. Moreover, the non-luminescent minerals illite, serpentine and talc also have high concentrations of $Fe^{3+}$ centres and almost no RID, a fact which favours the role of $Fe^{3+}$ as a luminescence quencher. If so, this would indicate that montmorillonite (high content of $Fe^{3+}$ centres) will also show no luminescence. However it is as yet not clear, whether there is a simple quenching by iron or a complex relationship between $Fe^{3+}$ centres, concentration of RID and luminescence intensity.

The origin of the CL emission at 580 nm, which is characteristic of halloysite and which was also detected in certain kaolinite samples, has also to be investigated further. Up to now there is no clear link to a specific defect or activator ion, which may be responsible for this luminescence.

## Conclusions

The minerals kaolinite, dickite, nacrite, halloysite and pyrophyllite are characterized by a deep blue CL, which is caused by a broad emission band around 400 nm.

The results of CL studies (wavelength/energy of the CL emission) as well as the behaviour under the electron beam and the results of the EPR measurements indicate that intrinsic electron-hole defects in the structure (RID centres) are responsible for the blue CL of the dioctahedral clay minerals. The origin of additional emission bands at 580 nm (halloysite, kaolinite) and in the red on the edge to the infrared (700–800 nm) is still unknown. The high concentration of $Fe^{3+}$ (that probably acts as luminescence quencher) and the low concentration of RID could explain the absence of visible CL from illite, serpentine and talc and may also indicate that montmorillonite would show no CL.

The results of the study also emphasize the role of sample preparation. The use of polished thin sections of powder samples prepared with epoxy resin led to a distortion of the spectral CL measurements. A broad emission from the epoxy resin between 450 and 650 nm has been detected, which prevents the spectral analysis in this region. The preparation of pressed tablets of powder samples and the analysis by spectral SEM-CL provided pure spectra of the clay minerals.

The characteristic luminescence behaviour of clay minerals can be applied in several fields of sedimentary petrology, sandstone petrography, petroleum exploration, alteration of crystalline rocks and investigations of building stones. The clay minerals kaolinite, dickite, nacrite and pyrophyllite are rapidly detectable due to their characteristic deep blue CL. We stress that it is now possible to differentiate between kaolinite and dickite by spectral CL, even in thin section. A recognition of nacrite is in most cases possible based on morphological criteria, whereas pyrophyllite can be distinguished from the two-layer sheet silicates by the differing Al:Si ratio.

## Acknowledgements

*U. Kempe* (Freiberg) is gratefully acknowledged for spectral SEM-CL measurements and *A. Renno* (Freiberg) for his help during preparation of pressed sample tablets. This research was funded by the Deutsche Forschungsgemeinschaft (DFG-grant No. GO 677/5-1). Review and editorial comments by *V. Correcher*, *M. Hodson* and *A. Finch* are very much appreciated.

## References

*Bailey SW* (1988) Hydrous phyllosilicates. Mineralogical Society of America, Washington DC (Rev Mineral 19)

*Chipera SJ, Bish DL* (2001) Baseline studies of the clay minerals society source clays: powder X-ray diffraction analyses. Clays Clay Miner 49: 398–409

*Clozel B, Allard T, Muller J-P* (1994) Nature and stability of radiation induced defects in natural kaolinites: new results and a reappraisal of published works. Clays Clay Miner 42: 657–666

*Görz H, Bhalla RJRSB, White EW* (1970) Detailed cathodoluminescence characterization of common silicates. In: *Weber JN, White EW* (eds) Space science applications of solid state luminescence phenomena. Penn State Univ Spec Pub 70–101: 62–70

*Götze J, Magnus M* (1997) Quantitative determination of mineral abundance in geological samples using combined cathodoluminescence microscopy and image analysis. Eur J Mineral 9: 1207–1215

*Götze J, Plötze M* (2000) Kathodolumineszenz von Kaolinit: Ursachen, Besonderheiten und praktische Anwendungen. Ber Dt Ton- Tonmineralgruppe 7: 92–99

*Gournis D, Mantaka-Marketou AE, Karakassides MA, Petridis D* (2000) Effect of $\gamma$-irradiation on clays and organoclays: a Mössbauer and XRD study. Phys Chem Minerals 27: 514–521

*Hinckley DN* (1963) Variability in ''crystallinity'' values among the kaolin deposits of the coastal plain of Georgia and South Carolina. Clays Clay Miner 11: 229–235

*Kogel JE, Lewis SA* (2001) Baseline studies of the clay minerals society source clays: chemical analysis by inductively coupled plasma-mass spectroscopy (ICP-MS). Clays Clay Miner 49: 387–392

*Marfunin AS* (1979) Spectroscopy, luminescence and radiation centres in minerals. Springer, Berlin Heidelberg New York, 352pp

*Marshall DJ* (1988) Cathodoluminescence of geological materials. Unwin Hyman, London, 146pp

*Meads RE, Malden PJ* (1975) Electron spin resonance in natural kaolinites containing $Fe^{3+}$ and other transition metal ions. Clay Miner 15: 1–13

*Mermut AR, Cano AF* (2001) Baseline studies of the clay minerals society source clays: chemical analysis of major elements. Clays Clay Miner 49: 381–386

*Müller-Vonmoos M, Kahr G* (1983) Mineralogische Untersuchungen von Wyoming Bentonit MX-80 und Montigel. NTB 83-12, Nagra, Hardstrasse 73, CH-5430 Wettingen, Switzerland

*Müller-Vonmoos M, Bucher F, Kahr G, Madsen F, Mayor P-A* (1991) Wechsellagerungen und Quellverhalten von Kalium-Bentonite. NTB 91-13, Nagra, Hardstrasse 73, CH-5430 Wettingen, Switzerland

*Neuser RD, Bruhn F, Götze J, Habermann D, Richter DK* (1995) Kathodolumineszenz: Methodik und Anwendung. Zbl Geol Paläont Teil I, H 1/2: 287–306

*Pagel M, Barbin V, Blanc P, Ohnenstetter D* (eds) (2000) Cathodoluminescence in geosciences. Springer, Berlin Heidelberg New York Tokyo, 514pp

*Plötze M, Kahr G* (2001) Alteration of clay minerals – influence of ionizing radiation. Ber Dtsch Ton- Tonmineralgruppe 8: 170–177

*Rene M, Götze J, Kempe U, Wolf D* (2001) Magmatic and metasomatic processes in albite granites of the Vysoky Kamen Cupola, Czech Republic. Cathodoluminescence in geosciences: new insights from CL in combination with other techniques. Abstracts, pp 106–107

*Weber J* (2000) Kieselsäurediagenese und gekoppelte Sedimentarchitektur – eine Beckenanalyse des Reinhardswald-Troges (Norddeutsches Becken, Solling-Folge, Mittlerer Buntsandstein). Kölner Forum Geologie Paläontologie 7: 3–165

Authors' addresses: Dr. *J. Götze* (corresponding author), TU Bergakademie Freiberg, Department of Mineralogy, Brennhausgasse 14, D-09596 Freiberg, Federal Republic of Germany, e-mail: goetze@mineral.tu-freiberg.de; Dr. *M. Plötze*, ETH Zürich, Department of Geotechniques, IGT ClayLab, CH-8093 Zürich, Switzerland; Dipl.-Geol. *Th. Götte,* Dr. *R. D. Neuser*, and Prof. Dr. *D. K. Richter*, Ruhr-Universität-Bochum, Department of Geology, Mineralogy, Geophysics, Universitätsstrasse 150, D-44801 Bochum, Federal Republic of Germany